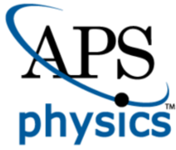

CHORUS

This is the accepted manuscript made available via CHORUS. The article has been published as:

Interfacial Bonding and Structure of Bi_{2}Te_{3} Topological Insulator Films on Si(111) Determined by Surface X-Ray Scattering

Y. Liu, H.-H. Wang, G. Bian, Z. Zhang, S. S. Lee, P. A. Fenter, J. Z. Tischler, H. Hong, and T.-C. Chiang

Phys. Rev. Lett. **110**, 226103 — Published 30 May 2013

DOI: 10.1103/PhysRevLett.110.226103

Interfacial Bonding and Structure of Bi_2Te_3 Topological Insulator Films on Si(111) Determined by Surface X-ray Scattering

Y. Liu[1,2*], H.-H. Wang[2,3], G. Bian[2], Z. Zhang[1], S. S. Lee[4], P. A. Fenter[4], J. Z. Tischler[1], H. Hong[1], and T.-C. Chiang[2*]

[1]Advanced Photon Source, Argonne National Laboratory, 9700 South Cass Avenue, Argonne, Illinois 60439, USA

[2]Department of Physics and Frederick Seitz Materials Research Laboratory, University of Illinois at Urbana-Champaign, Urbana, Illinois 61801, USA

[3]Institute of High Energy Physics, Chinese Academy of Sciences, Beijing 100049, China

[4]Chemical Science Division, Argonne National Laboratory, 9700 South Cass Avenue, Argonne, Illinois 60439, USA

[*]Corresponding authors: Y. Liu (yangliu3@aps.anl.gov), T.-C. Chiang (tcchiang@illinois.edu)

Interfacial topological states are a key element of interest for topological insulator thin films, and their properties can depend sensitively on the atomic bonding configuration. We employ *in situ* non-resonant and resonant surface X-ray scattering to study the interfacial and internal structure of a prototypical topological film system: Bi_2Te_3 grown on Si(111). The results reveal a Te-dominated buffer layer, a large interfacial spacing, and a slightly relaxed and partially strained bottom quintuple layer of an otherwise properly stacked bulk-like Bi_2Te_3 film. The presence of the buffer layer indicates a nontrivial process of interface formation and a mechanism for electronic decoupling between the topological film and the Si(111) substrate.

PACS numbers: 68.55.aj 73.61.Ng 68.35.Ct

The recent discovery of topological insulators (TIs) has sparked widespread interest in this new phase of matter [1,2,3,4]. A hallmark of TIs is the topological surface states (TSSs), which have been studied in detail by surface-sensitive techniques, most notably angle-resolved photoemission spectroscopy [5,6,7] and scanning tunneling microscopy [8,9]. While rapid progress has been made in understanding the vacuum-terminated surface of these materials, it is still challenging to probe experimentally the properties of the buried interface between a TI film and its underlying substrate. Yet the buried interface can be more important than the exposed surface. It is protected against the ambient environment, easily amenable to charge or voltage tuning, and is much better suited for device architecture and applications. More generally, tailored interfacial configurations could support a variety of novel electronic states [10,11]. Being able to precisely determine the interfacial atomic structure is a key step toward interfacial engineering and control.

Numerous transport measurements of films of the best known TIs, Bi_2Se_3 and Bi_2Te_3, have indicated enhanced surface conduction relative to the bulk samples [12,13,14,15]. When these films become very thin, quantum tunneling may link the surface and interface, resulting in a tunneling gap in the TSSs and hence rendering the system insulating [16]. Experimentally, tunneling gaps in Bi_2Te_3 and Bi_2Se_3 thin films vanish at 4 and 6 quintuple layers (QLs), respectively, in reasonable agreement with theoretical predictions for freestanding films [16,17,18,19]. By sharp contrast, Sb films grown on Si(111) exhibit a zero tunneling gap already at 4 bilayers despite a sizeable gap predicted by theory for a freestanding film [20]. These results illustrate that the overall electronic structure of the film-substrate system is material-specific and can be very sensitive to the atomic structure at the interface.

Here, we present a detailed study of the interfacial atomic structure of Bi_2Te_3 thin films grown on Si(111) using surface X-ray scattering, and discuss how the nontrivial structure affects the electronic properties. X-ray scattering is non-invasive with a large probing depth well suited for investigating buried structures [21]. We performed non-resonant and resonant X-ray scattering for element-sensitive mapping of the layer structure [22]. Previous structural determinations of TI films were mostly based on *ex situ* X-ray measurements in air, which explored issues of crystallinity and film thickness but did not probe the structure at atomic-scale resolution [23,24]. Our measurements were, instead, performed *in situ* under ultrahigh vacuum in order to avoid surface contamination that can become problematic for ultrathin films. The Bi_2Te_3 films were grown on a clean (7×7) reconstructed Si(111) surface under a Te-rich condition [17,18]. All X-ray measurements were performed at room temperature at sector 33-ID-E, Advanced Photon Source [25].

A schematic diagram of the experimental configuration is shown in Fig. 1(a), where a hexagonal surface coordinate system is used [26]. Figure 1(b) shows measured real-time anti-Bragg oscillations of Bi_2Te_3 during growth. The intensity increases rapidly to a maximum at a nominal film thickness of ~0.2 QL, after which it undergoes damped bi-QL oscillations. The sharp peak at 0.2 QL is unusual and indicates a nontrivial growth mode. It is attributed to the formation of a buffer layer based on additional evidences to be presented below and elsewhere [27]. The ensuing bi-QL oscillations indicate QL-by-QL growth above the buffer layer. Layer-by-layer growth is ordinarily characterized by intensity maxima at $2n + 1$ (odd layers), but interference from the buffer layer and substrate could influence the phase of oscillations [27].

The measured specular reflectivity from the (7×7) substrate and buffer-capped surface (0.2 QL coverage) is shown in Fig. 1(c). In regions away from the Si Bragg peaks at $L = 3$ and 9,

the reflectivity increases substantially with the addition of the buffer layer. Fitting of the data reveals a buffer layer sitting at ~2.7 Å above the top Si layer. This buffer layer has a (7×7) structure commensurate with the Si(111)-(7×7) substrate, as evidenced by simultaneous intensity increases for all of the 1/7 fractional peaks in in-plane scans; an example of K-scan at $H = 0$ and $L = 0.2$ is shown in Fig. 1(d). Further deposition beyond 0.2 QL results in intensity increases only at $K \sim 0.87$ and 1.74, indicating formation of a 1×1 Bi_2Te_3 film. A close inspection of the peak at $K \sim 0.87$ [inset in Fig. 1(d)] reveals, actually, two closely spaced peaks at $K = 0.86$ and 0.88, which correspond to the Si 6/7 fractional peak and the bulk Bi_2Te_3 peak, respectively. Evidently, this near-6/7 fractional match determines the epitaxial relationship. The intensities of both peaks grow from 0.2 to 1 + 0.2 QL, but further deposition of another QL results in increase of the bulk Bi_2Te_3 peak only. A similar behavior is observed for the peak near $K = 1.74$. Thus, the first QL is partially strained by the substrate, and additional QLs assume the bulk structure within the plane [27]. The sample configuration at 1 + 0.2 QL is shown schematically in Fig. 1(e).

Information about the interfacial atomic layer stacking for the 1 + 0.2 QL film can be extracted from the reflectivity data shown in Fig. 2(a). The interference fringes, with an average spacing of $\Delta L \sim 1$ ($\Delta q_z = 0.668$ Å^{-1}), correspond to a total film thickness of ~$2\pi/0.668 = 9.4$ Å. This is much larger than the spacing between the top and bottom Te layers in a QL (7.55 Å). Thus, the simple scenario, in which a QL film grows directly on the Si substrate, can be ruled out. For comparison, Fig. 2(a) presents model calculations for various scenarios. A model with a buffer layer between the QL and the substrate shows the correct interference features. Other models without a buffer layer or with the buffer layer placed atop the QL do not work.

This still leaves the question regarding the elemental distribution within the film. To address this issue, we employ resonant scattering using four photon energies to measure the

reflectivity: 13.294 keV (125 eV below the Bi L_3 edge), 13.419 keV (at edge), 13.544 keV (125 eV above edge), and 19.9 keV (away from edge) [Fig. 2(c), with the same common intensity scale]. The strongest resonant signal (or contrast) occurs near $L \sim 2.3$ and 4.4, indicating a dominant Bi layer spacing of ~2π/0.668/2.25 = 4.18 Å as expected for a QL. The four scans are fit simultaneously assuming a buffer layer under the QL film; the results are shown in Fig. 2(c). For a better comparison, both the data and the fits are also plotted in Fig. 2(b), with vertical offsets to separate out the scans. The agreement is excellent with the fitting χ^2 of 1.4. Additional evidence, including a model-independent analysis of the resonant scattering data, further confirms the model [27]. The element-specific electron density profile extracted from the fits is shown in Fig. 2(d). The buffer layer is dominated by Te, and the QL film above the buffer layer has a stacking structure very close to the bulk form. The distance between the buffer layer and the top Si layer is again ~2.7 Å, consistent with the results obtained earlier [Fig. 1(c)]. Thus, a buffer layer wets or terminates the Si(111)-(7×7) substrate prior to the formation of the Bi_2Te_3 film.

Similar resonant scattering experiments were performed on thicker films. An example is presented in Fig. 3 for a 5-QL film over a buffered Si(111), with the coverage determined by anti-Bragg intensity oscillations [Fig. 1(b)]. Despite the complex structure factor of Bi and the general phase issue [28], a strong resonant signal (or contrast) at $L = 1.9$, 2.8, and 3.7 indicates a periodicity of ~10.45 Å for the Bi, in qualitative agreement with the expected QL spacing (with two Bi atomic layers per QL). As before, the data are fit simultaneously, and the results [Fig. 3(b)] are in excellent agreement with the data, as demonstrated by the comparison in Fig. 3(a) with the separate scans vertically offset for clarity. Specifically, the strong resonant features near

L = 1.9, 2.8, and 3.7 are well reproduced. The extracted element-specific electron density profile [Fig. 3(c)] is consistent with bulk-like Bi_2Te_3 films over a Te-dominated buffer layer.

Further refinement and confirmation of the film structure is performed by simultaneously fitting the non-resonant reflectivity data taken over a wide range of momentum transfer for a number of different film thicknesses [Fig. 4(a)]. The analysis begins with a basic model, which assumes a buffer layer and no lattice relaxation in the Bi_2Te_3 films. The occupancies of atomic layers within each QL are constrained to be the same (as a result of QL-by-QL growth), while the relative occupancies for different QLs are allowed to vary to account for the film morphology (roughness). The fitting, not shown here, can already explain all of the essential features in the reflectivity data with χ^2 = 14. Allowing the lattices of the bottom QL to relax, which is reasonable based on our detailed studies of the 1 + 0.2 QL film (Figs. 1 and 2), improves the fit and reduces the χ^2 to ~9. The results are summarized in Fig. 4, and the same structure model is also used in the fitting of Fig. 3. The fits agree well with the data including the many interference fringes with wide intensity variations. The occupancy distribution of the QLs in the films becomes broader as the film thickness increases (Fig. 4(b)). This roughness buildup is in agreement with the observed damping of the anti-Bragg intensity oscillations [Fig. 1(b)].

The final structural model and parameters for a thick film are summarized in Fig. 4(c). The top Si double layer relaxation is very slight. The buffer layer is mostly Te and is commensurate to the (7x7) substrate. The bottom QL is slightly relaxed and partially strained, and the rest of the film is bulklike. The existence of a buffer layer was suggested previously [29,30], but the detailed structure (including the buffer layer position, interfacial strain, and film relaxation) as well as the structural evolution as a function of film thickness is not available from these earlier studies. We have also tried fitting the data with additional structural parameters. For

example, first-principles calculations suggest that the topmost QL could contract by as much as ~0.3 Å towards the second topmost QL [31]. However, allowing the top QL to relax in the fitting yields a negligible relaxation. The difference between our experiment and theory might be related to uncertainties in theoretical calculations involving van der Waals bonding (between neighboring QLs). Prior low-energy electron diffraction (LEED) analysis of this system yields results that are consistent with our findings about the surface structure [32], but detailed interfacial structure is not available from LEED.

The presence of the buffer layer points to a nontrivial growth behavior. What is the driving mechanism for its formation? The inter-QL bonding in Bi_2Te_3 is largely van der Waals in nature. Direct growth of Bi_2Te_3 on the Si(111) surface would not satisfy the chemically active Si dangling bonds. Energetically, the Si atoms would prefer bonding to either Te or Bi to form strong, partially ionic covalent bonds. Due to the Te-rich growth condition, as well as a smaller atomic radius and a higher electronegativity of Te atom, Si-Te bonding should be favored. The Si(111) surface then becomes passivated, which would be conducive to the growth of van der Waals bonded Bi_2Te_3 QLs. The weak interfacial bonding is consistent with the rather large distance of 3.41 Å between the bottom Te atomic layer in the first QL and the Te buffer layer. This picture is also consistent with the weak structural relaxation for the bottom QL and the slight strain effect. The interfacial relaxation damps out quickly, and by the second QL, the structure becomes indistinguishable from the bulk.

One could argue that, because of the buffer layer, the Bi_2Te_3 film is largely decoupled from the substrate, both structurally and electronically. Indeed, our detailed first-principles simulations indicate that the electronic structure of Bi_2Te_3 films grown on Te-capped Si is essentially the same as that of freestanding films (Fig. S1 in [27]). The electronic decoupling

renders the interfacial topological state (nearly) identical to the one on the vacuum-terminated surface. The resulting (near) degeneracy of the states gives rise to a tunneling gap in the TSSs at low coverages, as observed by photoemission measurements [17,18]. Our simulations also suggest that films grown directly on Si without the Te buffer layer would exhibit gapless TSSs (with somewhat modified dispersion relations), due to breakdown of the surface-interface degeneracy [27].

In summary, our X-ray study of the growth of a prototypical topological insulator, Bi_2Te_3, on the most important electronic substrate material Si, reveals important insights. The growth is epitaxial with a near 6/7 fractional lattice match. The formation process of the interface is nontrivial, involving a Te buffer layer that keeps the Bi_2Te_3 film atop essentially bulk-like and largely decoupled from the substrate. This decoupling can be an important feature for the utility of interfacial topological states for applications. The interface would provide protection from the environment and yet exert minimal perturbation to the topological electronic structure. The resonant X-ray scattering method presented herein is a powerful probe of the structure and chemistry at buried interfaces. While the present work demonstrates a weakly bonded interface in a TI/semiconductor system, it will be interesting to perform a systematic analysis of other cases where the bonding might be strong, e.g., Sb films on Si(111) [20]. This type of work is essential for understanding the interplay between the topological electronic states and the interfacial atomic structure.

This work is supported by the U.S. Department of Energy, Office of Science, Office of Basic Energy Sciences, under Grant No. DE-FG02-07ER46383 (T.-C.C.), and Contract No. DE-AC02-06CH11357 (for operation of the Advanced Photon Source, and for P.F. and S.S.L. who are funded by the DOE/BES Geochemistry Research Program). We thank Dr. Christian

Schlepuetz, Dr. June Hyuk Lee and Dr. Ruqing Xu for assistance with experimental setup and Dr. Xiaoxiong Wang for sharing insights based on first-principles calculations.

References

[1] C. L. Kane and E. J. Mele, Phys. Rev. Lett. **95**, 146802 (2005).

[2] M. König *et al*., Science **318**, 766 (2007).

[3] M. Z. Hasan and C. L. Kane, Rev. Mod. Phys. **82**, 3045 (2010).

[4] X.-L. Qi and S.-C. Zhang, Rev. Mod. Phys. **83**, 1057 (2011).

[5] D. Hsieh *et al*., Nature **452**, 970 (2008).

[6] D. Hsieh *et al*., Science **323**, 919 (2009).

[7] Y. L. Chen *et al*., Science **325**, 178 (2009).

[8] P. Roushan *et al*., Nature **460**, 1106 (2009).

[9] Z. Alpichshev *et al*., Phys. Rev. Lett. **104**, 016401 (2010).

[10] X.-L. Qi, T. Hughes, and S.-C. Zhang, Phys. Rev. B **78**, 195424 (2008).

[11] L. Fu and C. L. Kane, Phys. Rev. Lett. **100**, 096407 (2008).

[12] H. Peng *et al*., Nature Mater. **9**, 225 (2010).

[13] D. Kong *et al*., Nature Nanotech. **6**, 705 (2011).

[14] H. Steinberg, D. R. Gardner, Y. S. Lee, and P. Jarillo-Herrero, Nano Lett. **10**, 5032 (2010).

[15] F. Xiu *et al*., Nature Nanotech. **6**, 216 (2011).

[16] Y. Zhang *et al*., Nature Phys. **6**, 584 (2010).

[17] Y. Y. Li *et al*., Adv. Mater. **22**, 4002 (2010).

[18] Y. Liu, G. Bian, T. Miller, M. Bissen, and T.-C. Chiang, Phys. Rev. B **85**, 195442 (2012).

[19] O. V. Yazyev, E. Kioupakis, J. E. Moore, and S. G. Louie, Phys. Rev. B **85**, 161101 (2011).

[20] G. Bian, X. Wang, Y. Liu, T. Miller, and T.-C. Chiang, Phys. Rev. Lett. **108**, 176401 (2012).

[21] I. K. Robinson and D. J. Tweet, Rep. Prog. Phys. **55**, 599 (1992).

[22] J. Als-Nielsen, and D. McMorrow, *Elements of Modern X-ray Physics* (Wiley, 2011), 2nd Edition.

[23] L. Zhang *et al*., Appl. Phys. Lett. **101**, 153105 (2012).

[24] X. Liu *et al*., Appl. Phys. Lett. **99**, 171903 (2011).

[25] H. Hong and T.-C. Chiang, *Nucl. Instrum. Methods Phys. Res. A* **572**, 942 (2007).

[26] I. K. Robinson, W. K. Waskiewicz, R. T. Tung, and J. Bohr, Phys. Rev. Lett. **57**, 2714 (1986).

[27] See supplementary document, which contains a theoretical analysis of the interfacial bonding effects on the electronic structure, additional X-ray diffraction data, and details of the data analysis methods.

[28] C. Park and P. A. Fenter, J. Appl. Crystal. **40**, 290 (2007).

[29] T. Shirasawa, J. Tsunoda, T. Hirahara, and T. Takahashi, Phys. Rev. B **87**, 075449 (2013).

[30] S. Borisova, J. Krumrain, M. Luysberg, G. Mussler, and D. Grützmacher, Cryst. Growth Des. **12**, 6098 (2012).

[31] G. Bian, X. Wang, unpublished.

[32] N. Fukui *et al*., Phys. Rev. B **85**, 115426 (2012).

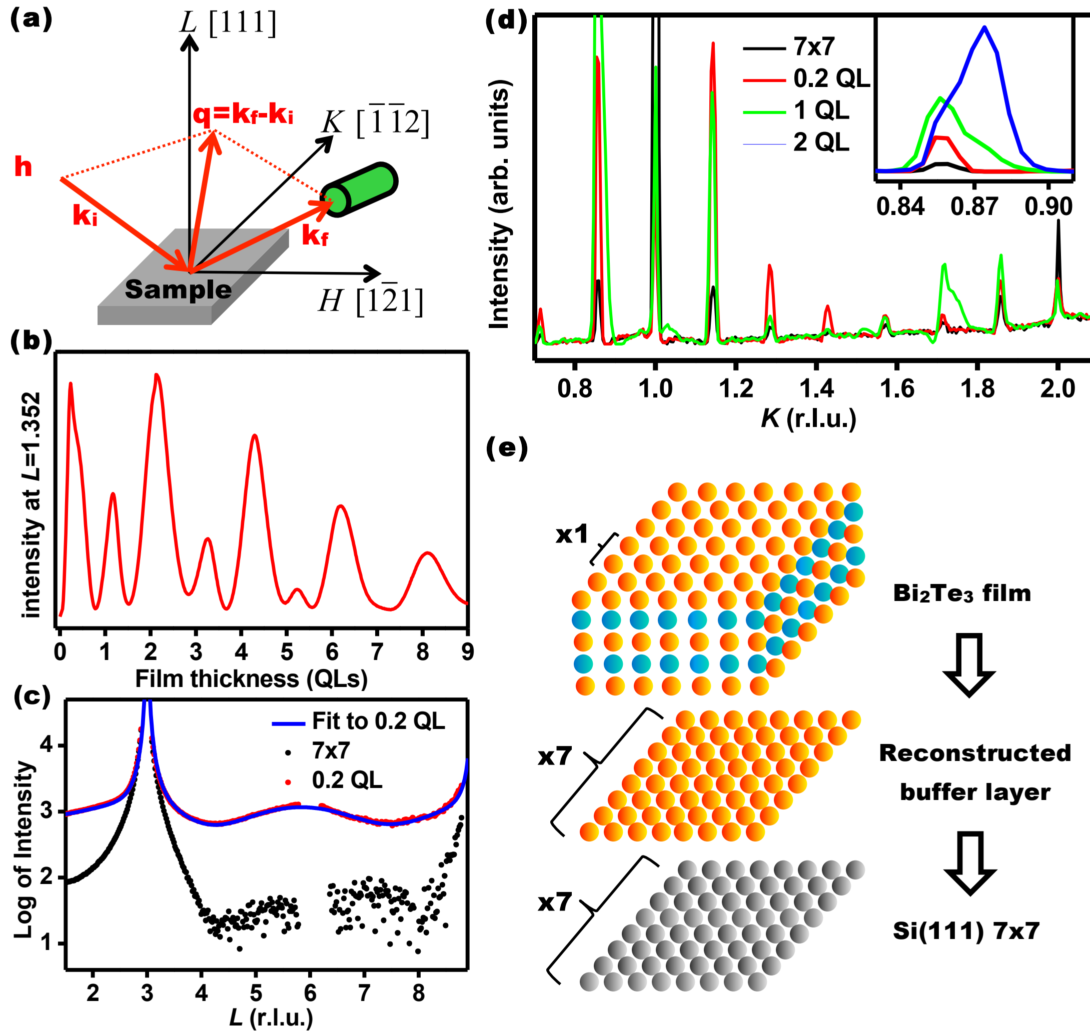

Fig. 1 (Color online). (a) Experimental geometry for surface X-ray scattering and the hexagonal surface coordinate system. $\mathbf{k}_i$, and $\mathbf{k}_f$ are the incident and reflected photon wave vectors. (b) Intensity oscillation at $(H, K, L) = (0, 0, 1.352)$ in Si reciprocal lattice units (r.l.u.) as a function of film thickness. The chosen L value is close to an anti-Bragg reflection of Bi_2Te_3. (c) Specular reflectivity data ($H = K = 0$) for the Si(111)-(7x7) surface (0 QL) and buffer-layer-capped surface (0.2 QL). A fit to the latter data set is shown. (d) A line scan along K ($H = 0$, $L = 0.2$) for the Si(111)-(7x7) surface, buffer-capped Si(111), and the same with the addition of 1 and 2 QLs. The inset shows the data near a bulk Bi_2Te_3 peak ($K = 0.88$), which is very close to the 6/7 fractional peak ($K = 0.86$) from the 7x7 reconstruction of Si(111). (e) Schematic atomic structure for the 1 + 0.2 QL film.

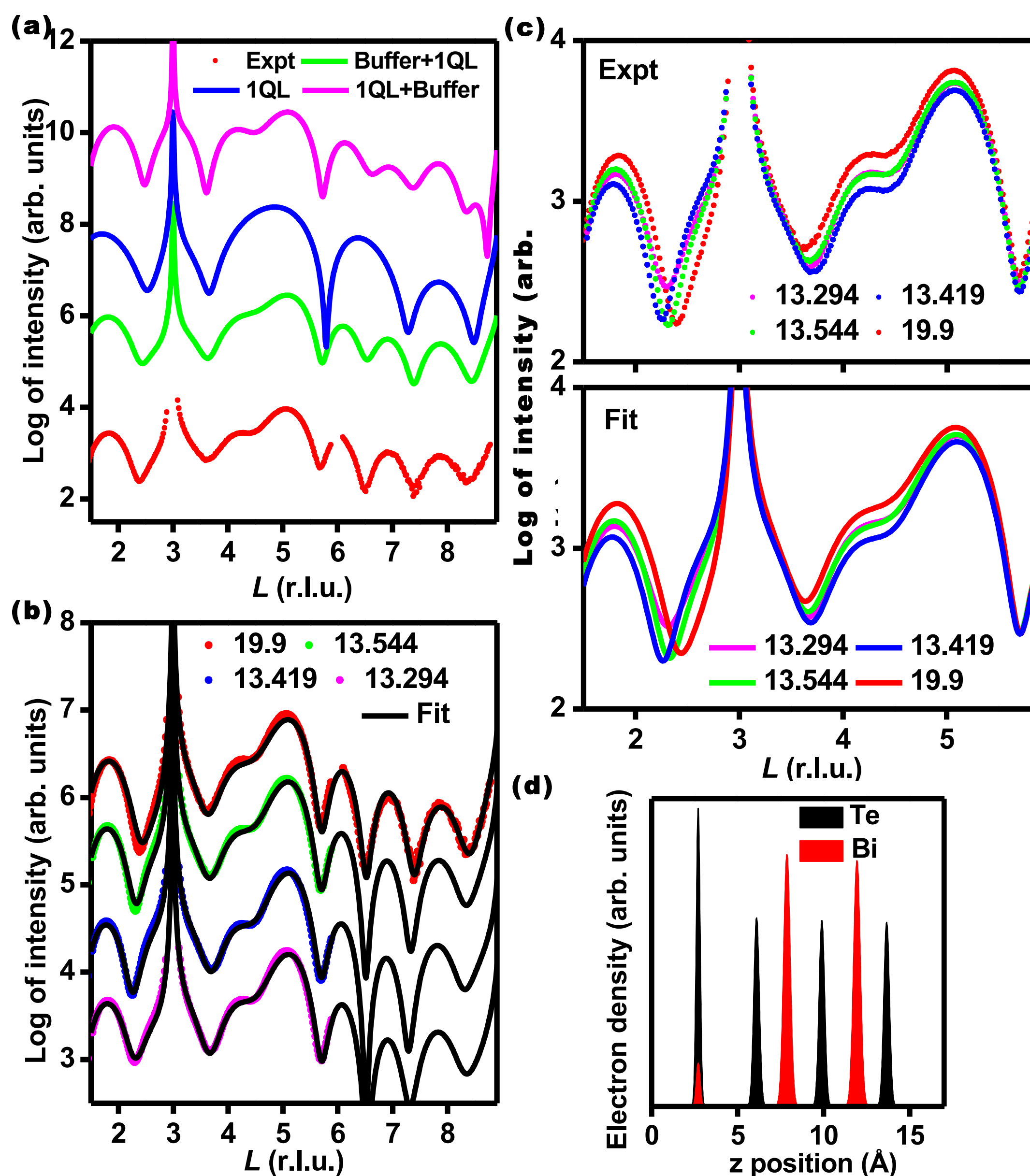

Fig. 2 (Color online). (a) Comparison of reflectivity data taken at 19.9 keV (red data points) with model calculations. Blue, green, and magenta curves are calculations for a 1-QL bulklike Bi_2Te_3 directly above the substrate (1 QL), a buffer layer in-between the film and substrate (buffer + 1 QL), and a buffer layer on top of the film (1 QL + buffer), respectively. (b) Reflectivity data for a 1-QL film taken at X-ray energies below, at, above, and far away from the Bi L_3 edge at 13.419 keV. The black curves are simultaneous fits. The curves in (a) and (b) are vertically offset for display clarity. (c) Data (top panel) and fitting results (bottom panel) without the offsets. The numbers in (b,c) indicate the corresponding photon energies in keV. (d) Deduced element-specific electron density profile; $z = 0$ is defined to be at the top Si atomic layer.

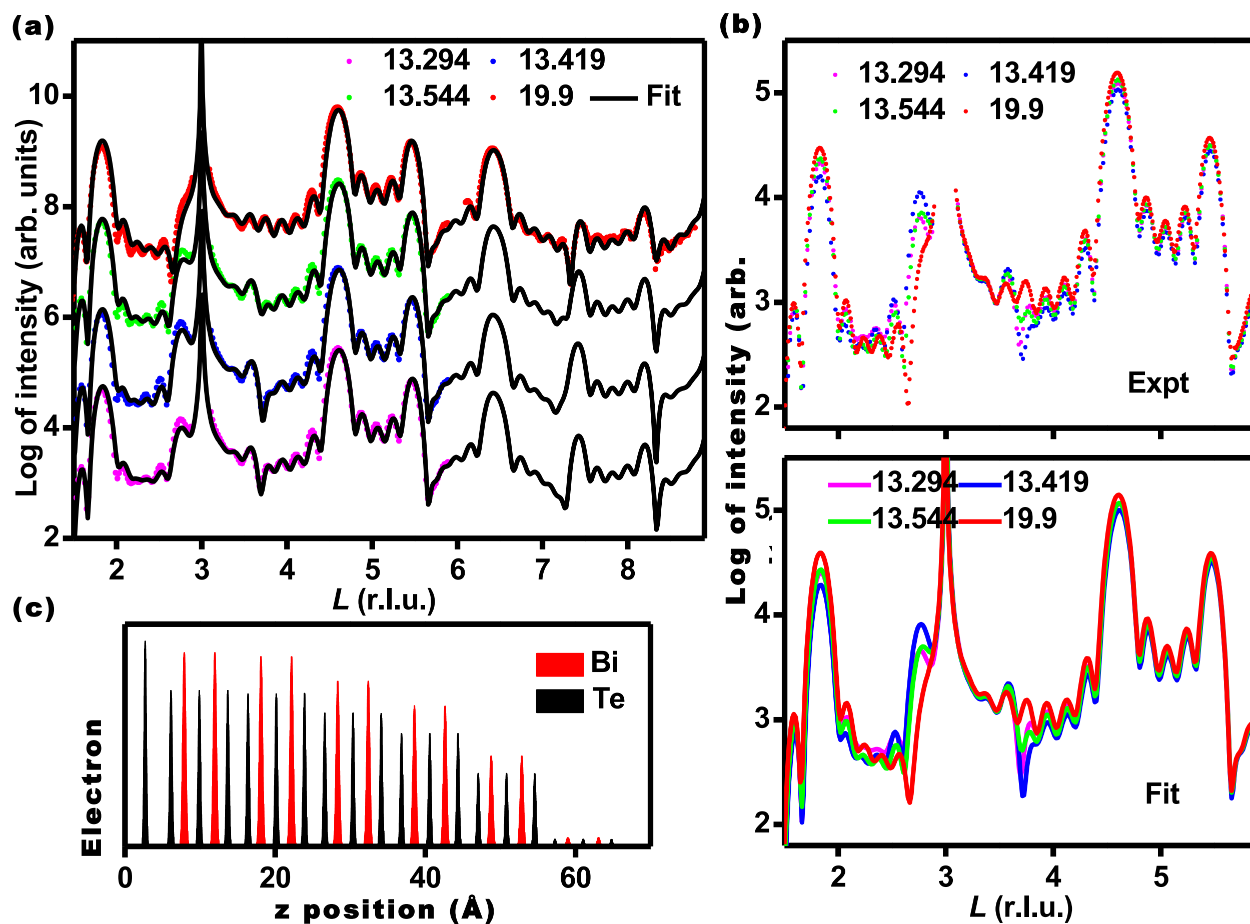

Fig. 3 (Color online). (a) Reflectivity data from a 5-QL film taken at X-ray energies below, at, above, and far away from the Bi L_3 edge (see caption of Fig. 2 for details), which are vertically offset for clarity. The black curves are simultaneous fits to the data. (b) Experimental data (top panel) and fitting (bottom panel) without the vertical offsets. (c) The element-specific electron density profile deduced from the fitting.

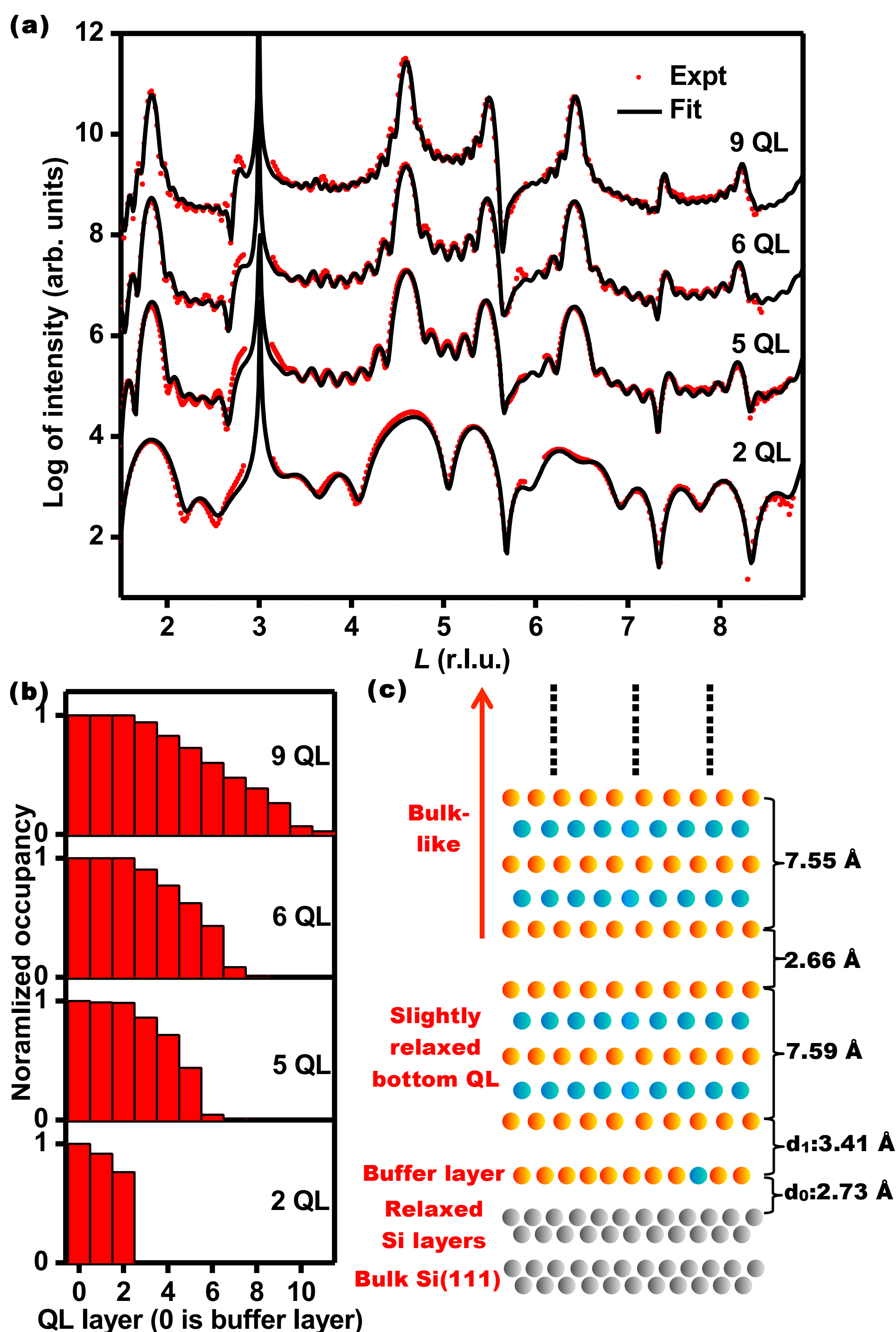

Fig. 4 (Color online). (a) Reflectivity data taken at 19.9 keV (red points) for various Bi_2Te_3 film thicknesses and model fits (black curves). The results are vertically offset for display clarity. (b) The resulting QL occupancy distribution for each film. Note that zero of the horizontal axis corresponds to the buffer layer. (c) Deduced atomic structure for a thick film.